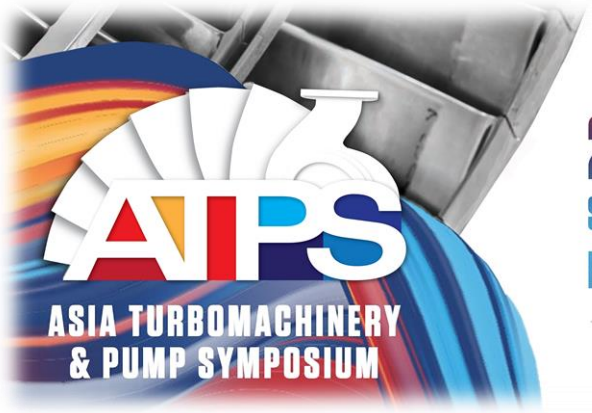

24-26 MAY 2022
SHORT COURSES: 23 MAY 2022
KUALA LUMPUR, MALAYSIA

ON THE INFLUENCE OF LUBRICANT FEEDHOLE SIZE AND END PLATE SEALS' CLEARANCE ON THE DYNAMIC PERFORMANCE OF INTEGRAL SQUEEZE FILM DAMPERS

Xueliang Lu
Bearings and Rotordynamics Expert
Technology Center
Hunan SUND Technological Corporation
Xiangtan, Hunan, China

Luis San Andrés
Mast-Childs Chair Professor
J. Mike Walker '66 Department of
Mechanical Engineering
Texas A&M University
College Station, TX, USA

Bonjin Koo
Product Development Engineer
Applied Development Center
Daikin Applied
Plymouth, MN, USA

Xueliang Lu received his B.S. and M.S. degrees in ME from Xiangtan University in China, and a PhD in ME at Texas A&M University under the supervision of Dr. San Andrés. Xueliang's research focused on the experimental identification and prediction of force coefficients for two phase flow seals and fluid film bearings. In 2017, the Structures and Dynamics Division of ASME-Turbo Expo recognized one of his papers, co-authored with Dr. San Andrés, as best in the field. After graduation, Xueliang worked for Atlas Copco as a lead mechanical engineer. In 2021, Dr. Lu joined Hunan Sund Technological Corp as a technology expert developing advanced rotor-bearing systems.

Luis San Andrés performs research in lubrication and rotordynamics and produced advanced technologies of hydrostatic bearings for cryogenic turbo pumps, squeeze film dampers for aircraft jet engines, and gas foil bearings for oil-free micro turbomachinery. Luis is a Fellow of ASME, GPPS, and STLE, and a member of the Industrial Advisory Committees for the Texas A&M Turbomachinery & Pump Symposia. Luis earned a MS in ME from the University of Pittsburgh and a PhD in ME from Texas A&M University. Luis has published over 260 papers in numerous ASME journals and conferences, including TPS and ATPS. Dr. San Andrés received the ASME 2022 Aircraft Engine Technology Award for sustained personal creative contributions to aircraft engine technology.

Bonjin Koo is a Product Development Engineer at Daikin Applied, a world leader in the HVAC compressors industry. He researches and develops high-speed rotor-bearing systems using fluid film bearings, ball bearings, and magnetic bearings. Bonjin earned BS and MS degrees in ME from Hanyang University in South Korea, and a PhD in ME from Texas A&M University under the guidance of Dr. San Andrés. Bonjin has authored several papers, some recognized as best in various technical conferences.

ABSTRACT

In rotating machinery, squeeze film dampers (SFDs) reduce rotor synchronous response amplitude motions, provide structural isolation and enhance rotordynamic stability. Compared to conventional squirrel cage supported SFDs, integral squeeze film dampers (ISFDs) are more compact and require a shorter axial span. This paper presents predictions of pressure profile, lubricant flow rate, and dynamic force coefficients of a four-arc pads ISFD having a diameter D= 141 mm, length L= 0.4 D, and clearance c =0.004 D; and configured with distinct inlet orifices (d_0 – 3 d_0, d_0=1.98 mm) and ends' seal gaps (b_1 - 3b_1, b_1 =0.191 mm = 1/3 c). The analysis quantifies the effect of the lubricant feedholes' size and the end seals' gap on the required flow and force coefficients of an ISFD for a typical compressor application. An increase in feed orifice diameter, from d_0 to 2d_0, rises significantly the fluid film pressure, delaying

the onset whirl speed of oil cavitation although demanding of more flow rate. Incidentally, for a nominal gap b_1 in the end plate seals, the ISFD damping and inertia coefficients reduce by almost 1/3 as the oil feed orifice diameter increases from d_0 to $2d_0$. The damping and inertia coefficients of the ISFD are more sensitive to the end seal clearance than to the diameter of the oil feed orifice. In addition, predictions for the ISFD operating with an air in oil mixture shows that the damping and added inertia coefficients drop almost linearly as the inlet gas volume fraction (GVF) increases from 0.0 (all liquid) to 0.2.

INTRODUCTION

The demand for high pressure and high aerodynamic efficiency continuously pushes a compressor/turbine to operate at ever-fast rotor speeds and with extremely tight clearances in the seals controlling secondary leakage paths. To keep the shaft surface speed at the support bearings under a reasonable limit, the journal diameter must reduce inversely to the increase in angular speed. The reduction in diameter makes the rotor more flexible when compared to the resilience of the journal bearings. Further, conventional gas seals such as labyrinth seals are prone to produce large cross-coupled stiffnesses for operation at high pressure (large gas density) while demanding of small clearance for leakage control. A flexible rotor plus large cross-coupled stiffnesses make conventional style fluid film bearings (both fixed pads or with tilting pads) inadequate to overcome rotor dynamic stability issues. In such a case, squeeze film dampers (SFDs) can be installed in series with the journal bearings to render a soft support that drops the system critical speeds while introducing additional damping to stabilize the rotor [1,2].

In 1996, Zeidan et al. [3] sum the characteristics of four types of SFDs; the ones without a centering spring being the simplest. This last type of SFD is at its bottom when the rotor start-ups; and as the shaft speed increases, the damper develops a centering like-stiffness due to persistent oil cavitation. Elastomeric O-rings are simple means to provide a centering stiffness and added damping in light weight rotors [3,4]. However, the stiffness of O-rings is difficult to predict as it varies with the elastomer material properties, the assembly compression, the compatibility with the lubricant, and the operating temperature and frequency. Aging is also a problem for O-ring sealed SFDs. Gooding et al. [5] report a vibration issue in a test facility to study aerodynamics of an overhung centrifugal compressor for aero-engine applications. The compressor installed with O-rings sealed SFDs stably operated for several years, but became unstable at a certain threshold speed as the years passed by. The authors suspect the degradation of the sealing O-rings reduced the effective length of the damper and lead to a decrease in the damper stiffness and damping coefficients. Squirrel cage supported SFDs are the most commonly used design in aircraft engines [3, 6]. The squirrel cage not only provide means to center the rotor, but also can be used to tune the system natural frequency as its stiffness is adjustable over a wide range. However, squirrel cages require a large axial space for installation and are difficult to center during the assembly process.

To overcome the difficulties of the aforementioned types of SFDs, Zeidan et al. [3] introduce a type of integral damper that features S-shaped flexible webs as centering springs. The electrical discharge machining (EDM) process makes the webs in the same piece of raw material as the damper ring. Thus, the centering spring and the SFD are integral to a single custom-made piece; hence then the name squeeze film damper (ISFD) [1]. Early versions of the ISFD mainly served to tune the natural frequency of the rotor-bearing system so as to improve the separation margin between running speed and critical speeds [7, 8]. Agnew and Childs [8] identify the force coefficients of a four-pad flexure pivot tilting pad journal bearing in series with an ISFD. The experimental results show that the ISFD-bearing has a lower direct stiffness and added mass coefficients compared to those of the tilting-pad bearing alone, and whereas the test system damping coefficient are practically the same.

ISFDs aided to stabilize otherwise unstable systems such as in steam turbines [9,10] and in a high-speed integrally geared centrifugal compressor [11]. Ertas et al. [10] discuss stabilizing a 46 MW multistage utility steam turbine (nominal speed 5500 rpm, rotor mass 6,320 kg) using ISFD supported bearings. The original design of the turbine had two 50% offset rocket pivot, five-pad, load on pad tilting pad journal bearings (TPJBs). During the initial commissioning, the turbine tripped with a high amplitude subsynchronous vibration (SSV) at 30 Hz (0.33X) when the power > 35 MW. A rotordynamic analysis shows that the flexible rotor plus the seal and turbine stage destabilizing forces [12, 13] yield a system with negative damping ratio at the first forward mode (~30 Hz). To solve the SSV issue, the authors introduced an ISFD and replaced the five-pad TPJBs with a four-pad, load between pads TPJBs. The series five-pad TPJB and ISFD has a direct stiffness 20% lower than the original TPJB. After the retrofit, the turbine operated stably (no SSV).

Since its invention in the early 1990s, ISFDs are recommended to ameliorate different types of vibration issues in rotor-bearing systems. However, there are very limited number of component level studies on the static and dynamic performance of ISFDs. Ertas et al. [14] measure and predict damping and inertia coefficients for a four pads ISFD with a diameter D=141 mm and axial length L=56 mm, and end plate seals' with various clearances. The authors find that the ISFD damping and inertia coefficients dramatically decrease as the gap in the seal increases. An experimental program conducted by Lu et al. [15] with a four pads ISFD shows similar trends in damping and inertia coefficients as the end seals' clearance increases. The test ISFD has diameter D=157 mm (L/D=0.48), pad arc extend =73^o, film clearance c=0.353 mm, and axial seal gap = 1.5c, 1.21c, and 0.8c. The damper with the tightest seals (gap=0.8c) produces a unique stiffness hardening as the excitation frequency increases. The large increase in dynamic stiffness is due to fluid compressibility.

As is well known, in conventional (cylindrical) 360^o SFDs, the oil feed conditions such as supply pressure and the number and diameter of feedholes affect the SFD damping and inertia coefficients. In 1996, Zhang and Roberts [16] analyze the effect of lubricant supply mechanism on the force coefficients of a centrally grooved, short length SFD, and find a nonzero fluid static force, which is

linearly related to the supply pressure. Later in 2017, San Andrés et al. [17] detail an experimental effort to quantify the similarities and differences in forced performance in a SFD sealed with either piston rings or O-rings. The damper has diameter D=127 mm (L/D=0.2), and clearance c=0.373 mm (c/D=0.003). Supplied with ISO VG 2 oil at just 0.6 bar-g, one or three holes, evenly positioned around the damper circumference, deliver fluid into the squeeze film land. The measurements show that the SFD having three feedholes produces 20% - 40% less damping compared to the SFD supplied with just one feedhole. The authors argue the feedholes disturb the film dynamic pressure field (also measured) and cause a reduction in damping.

Recently (2020), Iacobellis et al. [18] conducted experiments to study the effect of number of feedholes and mass imbalance on the response of a rotor supported on SFDS, with either sealed ends or with open ends. A ball bearing in series with a SFD supports the rotor at each end. The rotor weighing 20.8 kg turned to a maximum speed of 20 krpm and crossed a bending mode critical speed. Four equally spaced holes around the damper circumference feed lubricant at a supply pressure of 5.5 bar. The SFDs can operate with a combination of one to four (open) feedholes. For the same amount of imbalance, and when supported by the SFD with four feedholes (both the sealed and open ends), the rotor response is smaller in amplitude when crossing the critical speed. The rotor amplitudes of motion reveal the SFD with four feedholes generates more damping than the SFD with only one feedhole. This finding opposes the experimental results in Ref. [17] albeit the pressure supply in Ref. [18] is not practical. The authors argue that the SFD with four feedholes is less likely to draw air ingestion into the film lands because the damper with more feedholes demands substanially more flow.

The extensive research shows that both the inlet feed holes and end seal clearances greatly affect the dynamic force coefficients of conventional SFDs. However, there is very scant literature on the influence of feedhole size and disposition on the dynamic forced performance of ISFDs. Therefore, this lecture provides insight on how the supply oil flow rate, pressure profile and dynamic force coefficients change with the diameter of inlet feed orifices and end seal clearances.

ANALYSIS

Figure 1 shows a schematic view of an integral squeeze film damper [15]. Four pairs of S-springs connect the damper outer ring to the inner ring that supports the housing of a roller element bearing or a fluid film bearing. The damper pads have arcuate extent Θ_p and are supplied with lubricant through a feedhole at the pad mid plane. The graph includes a coordinate system (x, y) with the angle Θ starting from the $-x$ axis. Undergoing a circular centered orbit (CCO) with amplitude r_o and frequency ω, the displacement vector of the center of the inner ring is [19]

$$\mathbf{z} = \begin{bmatrix} e_{sX}(t) \\ e_{sY}(t) \end{bmatrix} = r_o \begin{bmatrix} \cos(\omega t) \\ \sin(\omega t) \end{bmatrix} \tag{1}$$

Accordingly, the film thickness $h(t)$ in the segments of the integral squeeze film damper is

$$h_{(t)} = c + e_{sX(t)} \cos(\Theta) + e_{sY(t)} \sin(\Theta) \tag{2}$$

where c is the nominal radial clearance produced by the electrical discharge manufacturing (EDM) process. The first and second time derivatives of the film thickness are

$$\dot{h}_{(t)} = \dot{e}_{sX_{(t)}} \cos(\Theta) + \dot{e}_{sY_{(t)}} \sin(\Theta) \tag{3}$$

$$\ddot{h}_{(t)} = \ddot{e}_{sX_{(t)}} \cos(\Theta) + \ddot{e}_{sY_{(t)}} \sin(\Theta) \tag{4}$$

where $\begin{bmatrix} \dot{e}_{sX} \\ \dot{e}_{sY} \end{bmatrix} = r_o \omega \begin{bmatrix} -\sin(\omega t) \\ \cos(\omega t) \end{bmatrix}$, and $\begin{bmatrix} \ddot{e}_{sX} \\ \ddot{e}_{sY} \end{bmatrix} = -r_o \omega^2 \begin{bmatrix} \cos(\omega t) \\ \sin(\omega t) \end{bmatrix}$.

Figure 2 shows a cross section view of the ISFD with side ends sealed with end plates with radial length l_1 and axial gap b_1. Each damper segment features an orifice with diameter d_0 to deliver lubricant into the mid plane of the arcuate fluid film land. As shown in the graph, the lubricant enters the orifice at supply pressure[1] P_s, and flows across the orifice to enter a film land at pressure P_i. After exiting the film land with pressure P_e, the lubricant flows through the gap between the end plates and the outer ring and discharges to ambient at pressure P_a.

1 In a centrifugal compressor, a typical range for the oil supply pressure is 1.7 to 3.5 bar-g.

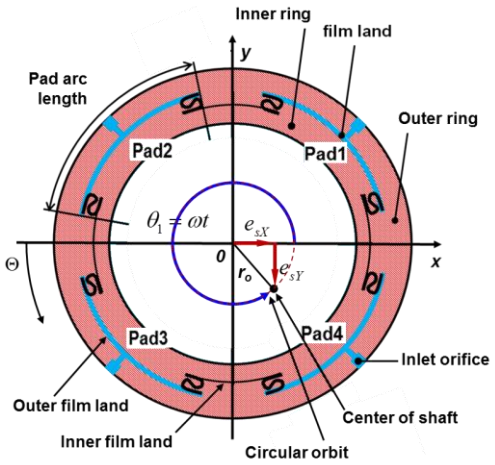

Figure 1 Schematic view of an integral squeeze film damper and coordinate system [15].

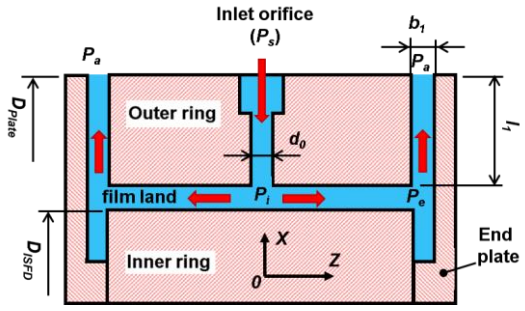

Figure 2 A cross section view of an ISFD showing the flow path: → orifice → film land → through gap of end plate seals [15].

Delgado and San Andrés [20] introduced an extended Reynolds Equation that includes temporal fluid inertia effects. The pressure field (p) in a film land is governed by:

$$\frac{\partial}{R\partial\Theta}\left(\frac{\rho h^3}{12\mu}\frac{\partial p}{R\partial\Theta}\right)+\frac{\partial}{\partial z}\left(\frac{\rho h^3}{12\mu}\frac{\partial p}{\partial z}\right)=\frac{\partial}{\partial t}(\rho h)+\frac{\rho h^2}{12\mu}\frac{\partial^2}{\partial t^2}(\rho h) \tag{5}$$

where μ and ρ are the lubricant viscosity and density, respectively. For operation with a two-phase flow (gas in oil mixture), the effective viscosity and density are:

$$\mu = \mu_g\alpha + \mu_l(1-\alpha) \tag{6}$$

$$\rho = \rho_g\alpha_g + \rho_l(1-\alpha) \tag{7}$$

with μ_g and μ_l , and ρ_g and ρ_l as the viscosity and density of the gas and liquid components, respectively, and α is the gas volume fraction (GVF). For a homogeneous mixture, the local gas volume fraction is a direct function of the film pressure [21]:

$$\alpha_{(p)} = \frac{1}{1+\dfrac{p_{(\Theta,z,t)}-P_v}{P_s-P_v}\left(\dfrac{1-\alpha_s}{\alpha_s}\right)} \tag{8}$$

where $P_v \sim 1$ kPa [21] is the liquid cavitation pressure, and α_s is gas volume fraction at a supply condition. As boundary conditions, note that at the two circumferential ends of the arcuate pads, the S-springs block the circumferential flow, i.e. ,

$$q_\theta \sim \frac{\partial p}{\partial\Theta} = 0 \tag{9}$$

The film axial ends ($z=\pm$½ L) can be either sealed or open to ambient. For an open ends condition, the lubricant exit pressure is ambient (P_a). For a sealed ends damper, the mass flow (q_{1z}) per unit circumferential length through the end seal is proportional to the local pressure drop and a local flow resistance [15],

$$q_{1z}\Big|_{\Theta,z=\pm\frac{1}{2}L} = -\frac{\rho h^3_{\left(z=\pm\frac{1}{2}L\right)}}{12\mu}\frac{\partial p}{\partial z}\bigg|_{z=\pm\frac{1}{2}L} = -\frac{\rho b_1^3}{12\mu l_1}(P_e-P_a) \tag{10}$$

Note that if $P_e > P_a$, the fluid flows from the damper film toward ambient; whereas if $P_e < P_a$, the flow reverses direction.

The mass of the lubricant flowing through a feed orifice with diameter d_0 is [19]

$$Q_{in} = \mathrm{sgn}(P_s-p_i)\left[C_f A_{eq}\sqrt{2\rho|P_s-p_i|}\right] \tag{11}$$

where C_f is an orifice discharge coefficient, and A_{eq} is an equivalent flow area. Ertas et al. [14] use $A_{eq} = A_0 \cdot A_c \Big/ \sqrt{A_0^2 + A_c^2}$ with $A_o = ¼\,\pi d_0^2$ and $A_c = \pi c\, d_0$. Ref. [14] uses $C_f = 0.98$ to match the predicted oil flow to the measured one.

The computational program developed implements a finite volume method (FVM) to iteratively solve the extended Reynolds Eq. (5). A difference of 1‰ or less between consecutive pressure fields determines convergence in the squeeze film land. A Newton-Raphson Method balances the lubricant flowing into/out of the damper arcuate pads.

Once the pressure field (p) is obtained, the fluid force (**F**) acting on the inner ring of the ISFD is [19]:

$$\begin{bmatrix} f_{X(t)} \\ f_{Y(t)} \end{bmatrix} = \tfrac{1}{2} D \sum_{j=1}^{n} \int_0^L \int_{\theta_1^j}^{\theta_2^j} p^j_{(\Theta,z)} \begin{bmatrix} \cos\Theta \\ \sin\Theta \end{bmatrix} d\Theta\, dz \tag{12}$$

where (θ_1^j , θ_2^j) denote the angles for the leading edge and trailing edge of the j_{th} pad, respectively.

The steps to numerically obtain the ISFD force coefficients; namely, stiffness (**K**), damping (**C)** and inertia (**M**) coefficients, are similar to those in the experimental procedure detailed in Ref. [22]. The inner ring of the ISFD whirls forward ($|\mathbf{z}|e^{i\omega t}$) and backward ($|\mathbf{z}|e^{-i\omega t}$) over a specified frequency range. Correspondingly, the forward and backward whirl motions produce reaction forces $|\mathbf{F}_+|e^{i\omega t}$ and $|\mathbf{F}_-|e^{-i\omega t}$. The whirl motions and the calculated reaction forces render the ISFD complex dynamic stiffness (**H**), from which linearized dynamic force coefficient are extracted, i.e.,

$$\mathbf{H}_{(\omega)} = \mathbf{F}_{(\omega)} \quad \mathbf{z}^{-1}_{(\omega)} \tag{13}$$

where $\mathbf{F}_{(\omega)} = [\mathbf{F}_{(+)} \mid \mathbf{F}_{(-)}]$, $\mathbf{z}_{(\omega)} = [\mathbf{z}_{(\omega)} \mid \mathbf{z}_{(-\omega)}]^{\mathrm{T}}$ are matrices with reaction forces and specified displacements, forward and backward. Re(**H**) and Ima(**H**) are the real and imaginary parts of the complex dynamic stiffness matrix. Then,

$$\text{Re}(\mathbf{H}) \rightarrow (\mathbf{K} - \omega^2 \mathbf{M}), \quad \text{Ima}(\mathbf{H}) \rightarrow (\omega \mathbf{C}) \tag{14}$$

from which the force coefficients (K,C,M) are extracted via curve fits of the functions over a frequency range.

PREDICTIONS AND COMPARISONS TO TEST DATA

ISFD pressure field and lubricant flow rate

Table 1 lists the main dimensions for the ISFD and the lubricant physical properties, as in Ertas et al. [14]. To conduct a complete parametric study on how the end seals' gap (b_1) and the size (d_0) of the inlet orifices affect the performance of the ISFD; this work also includes predictions for the same ISFD with end seals' clearance varying from b_1 to $3b_1$ and the orifice diameter increasing from d_0 to $3d_0$. For the prediction of force coefficients, the whirl frequency (ω) of the ISFD inner ring ranges from 20 Hz to 120 Hz, and the amplitude of the circular centered orbits (CCOs) increases from r_0=23 μm (4% c) to r_0=112 μm (20% c). The maximum squeeze film speed $v_s = \omega r_0 = 84.5$ mm/s, and the maximum squeeze film Reynolds number $Re_s = (\rho/\mu)\, \omega c^2 = 10.9$.

Table 1. Dimension of a sample ISFD and fluid properties [14].

Diameter at film land, D	141 mm
Length, L	56 mm
Film land clearance, c	0.56 mm
Number of pads, n	4
Pad arc extent Θ_p	54°
Feed orifice diameter, d_o	1.98 mm, 3.96 mm, 5.94 mm
End seals clearance, b_1	0.191 mm, 0.382 mm, 0.573 mm
radial length, l_1	5.1 mm
ISO VG32 Viscosity, μ_l	19.1 cP at 49 ºC
Density, ρ_l	871 kg/m^3
Supply pressure, P_s	2.4 bar(a)
Ambient pressure, P_a	1.0 bar(a)

Figure 3 shows the pressure profile in a single pad of a sealed ends ISFD supplied with Ps =2.4 bar(a) through orifices with d_0 = 0.198 mm and 0.396 mm. The damper is centered and the whirl frequency of the inner ring is null, i.e. a static condition. The pressure at the two side ends is above ambient due to the large flow resistance created by the tightness of the end seals (b_1=0.191 mm = 0.34 c). The ISFD with d_0 = 0.198 mm produces an orifice discharge pressure of 1.61 bar(a), whereas the ISFD *with the larger orifice* (less flow resistance) gives a larger discharge pressure of 2.03 bar(a) into the film land.

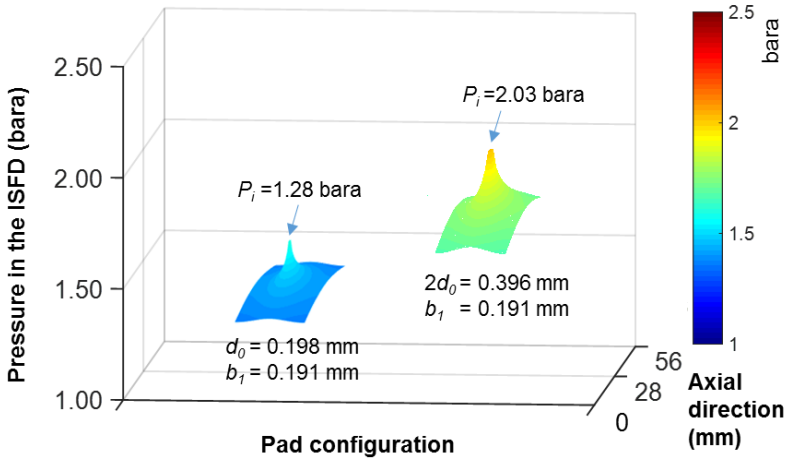

Figure 3 Pressure profiles in the film lands of a centered ISFD with sealed ends and two size oil feed orifices. Supply pressure P_s=2.4 bar, ambient pressure P_a=1.0 bar, whirl frequency ω=0 Hz.

Figure 4 depicts the ISFD oil flow rate versus supply pressure (P_s). The end seals' clearance is b_1=0.191 mm, and the diameter of the oil inlet orifice equals d_0 =1.98 mm, 2 d_0 and 3d_0. The lines denote predictions while the symbols represent the recorded data in Ref. [14]. As the diameter of the orifices increases from d_0 to 2d_0, the flow rate almost doubles. Note that API 614 [23] requires two to fifteen minutes of retention time in an oil reservoir[2] . The larger orifice diameter will inevitably increase capital expenditures as the larger supply flow calls for a larger volume reservoir.

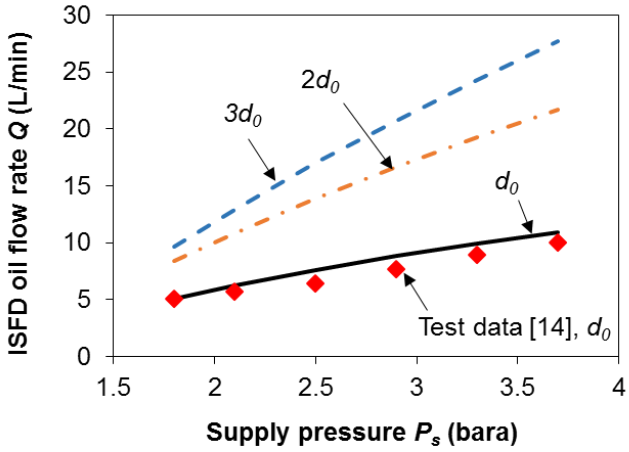

Figure 4 ISFD oil flow rate vs. supply absolute pressure (P_s). Lubricant orifice diameter varies, end seal b_1=0.191 mm. Comparisons to measured flow in Ref. [14].

Figure 5 shows pressure profiles in a pad of a sealed ends ISFD (b_1=0.191 mm, d_0 =1.98 mm) as the inner ring describes circular centered orbits (CCO) with amplitude r_0=56 μm (0.10 c). P_s=2.4 bar(a) and P_a=1.0 bar(a). The top graph shows the pressure field in pad 1 (see Figure 1 for reference) at the instant t =0 when the ring center dynamic displacement aligns with the +x axis, and the whirl frequency is 70 Hz (v_s=24.6 mm/s, Re_s=6.4). The bottom graph shows the pressure and film thickness versus normalized time (t/T) at z=¼ L and Θ = ½ Θ_p over one period of whirl motion (T=2π/ω). The curves denote operation with frequency ω = 70 Hz, 80 Hz (v_s=28.1 mm/s, Re_s=7.3), and 100 Hz (v_s =35.2 mm/s, Re_s=9.1). For operation at ω = 80 Hz, the pressure wave is close to the one for 0 bar(a) at t/T~0.3. As the whirl frequency of the inner ring reaches 100 Hz, the pressure is below the oil cavitation pressure during the time period t/T = 0.2~0.4.

2 The retention time is the amount of time that the lubricant stays in the oil reservoir before its return into the piping system. A typical retention time is between three to five minutes.

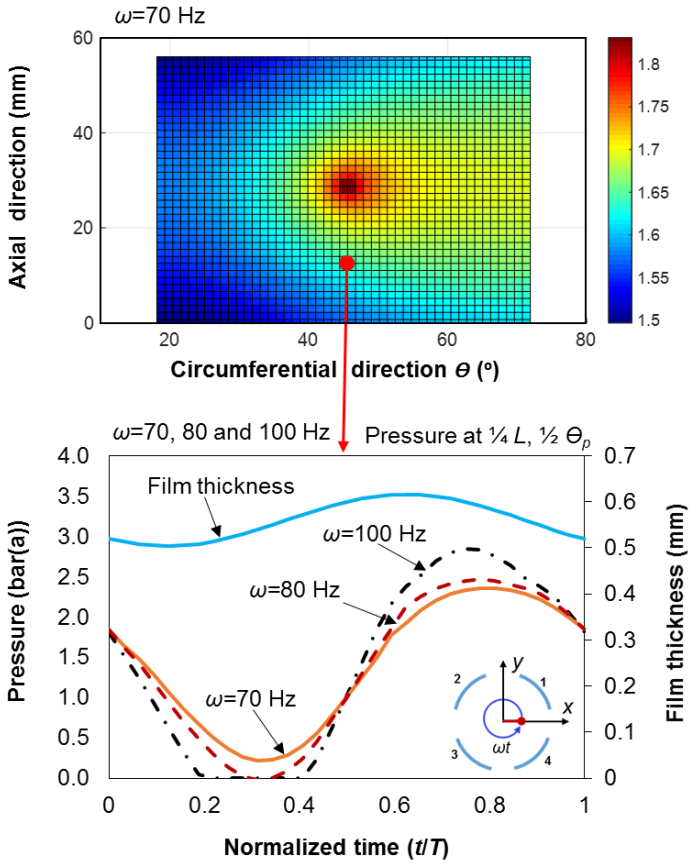

Figure 5 Top graph: snapshot of the pressure profile in a single pad (#1) at t=0 s (whirl frequency 70 Hz). Bottom graph: pressure and film thickness vs. normalized time (t/T) at z=¼ L and Θ = ½ Θ_p (whirl frequency 70 Hz, 80 Hz, and 100 Hz). Inlet orifice diameter = d_0. End seals' clearance b_1 = 0.191 mm. Supply pressure P_s=2.4 bar(a), ambient pressure P_a=1.0 bar(a), amplitude of whirl motion r_0 = 10% c.

ISFD dynamic force coefficients

Figure **6** shows the predicted complex dynamic stiffness, Re(H_{XX}) and Ima(H_{XX}), vs. whirl frequency (ω). The gap of the end seals b_1=0.191 mm, whereas the feed orifice diameter = d_0, 2 d_0 and 3d_0. The amplitude of whirl motion is r_0=0.1 c. Note the predictions produce H_{XX} = H_{YY}. Re(H_{XX}) is a parabolic function of frequency (ω), except for the configuration having d_0= 1.98 mm. Thus, Re(H_{XX}) can be characterized with a static stiffness (K) and a virtual mass (M), i.e., Re(H_{XX}) → (K-$\omega^2 M$). The fluid films in the ISFD do not produce a significant static stiffness as P_s=2.4 bar(a) is low. The increase in orifice diameter from d_0 to 3d_0 causes Re(H_{XX}) to reduce less with frequency.

The imaginary part of H_{XX} is a linear function of frequency and reducing in magnitude as the orifice diameter increases. Recall that for the ISFD with d_0=1.98 mm, oil vapor cavitation occurs when ω > 80 Hz (ωr_0=28.1 mm/s). Thus, the curve representing Ima(H_{XX}) reaches a turning point at ω=80 Hz. Note that the increase in orifice diameter from d_0 to 2 d_0 removes the turning point of Ima(H_{XX}), indicating that the onset of oil vapor cavitation is delayed to a higher whirl frequency.

Figure **7** shows the real and imaginary parts of the cross coupled complex dynamic stiffness (H_{XY})vs. frequency. The predictions deliver H_{XY} = - H_{YX}, and for simplicity, only H_{XY} is shown. Compared to the direct coefficient H_{XX}, H_{XY} is very small in magnitude. For the ISFD with orifice diameter d_0, Re(H_{XY}) switches from positive to negative at high frequencies, and Ima(H_{XY}) becomes nonlinear at high frequencies where oil vapor cavitation occurs in the fluid film.

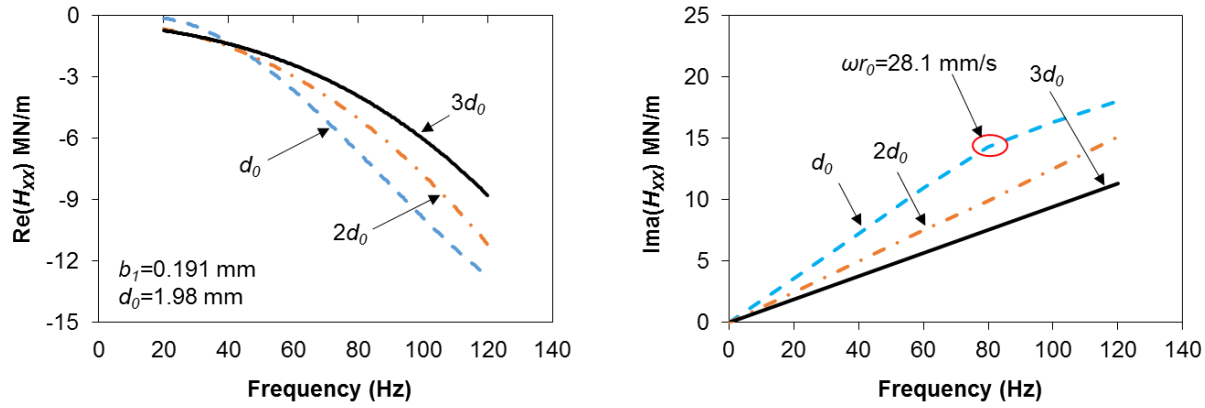

(a) Re(H_{XX}) **(b) Ima(H_{XX})**

Figure 6 Direct complex stiffness H_{XX}=H_{YY} vs. frequency. Real and imaginary parts. Inlet orifice diameter = d_0 , $2d_0$, and $3d_0$. End seals' clearance b_1=0.191 mm. P_s=2.4 bar(a), P_a=1.0 bar(a), amplitude of whirl motion r_0=0.1 c.

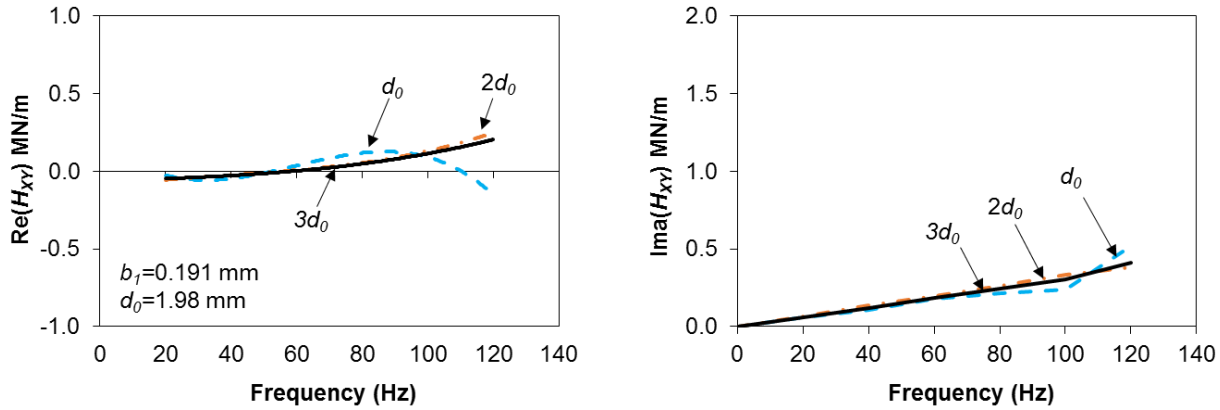

(a) Re(H_{XY}) **(b) Ima(H_{XY})**

Figure 7 Cross coupled complex stiffness H_{XY} = - H_{YX}. vs. whirl frequency. Real and imaginary parts. Inlet orifice diameter = d_0 , $2d_0$, and $3d_0$. End seals' clearance b_1=0.191 mm. P_s=2.4 bar(a), P_a=1.0 bar(a), amplitude of whirl motion r_0=0.1 c.

Figure 8 depicts the direct damping coefficient (C) derived from a linear curve fit of Ima(H_{XX}) vs. end seal clearance b_1 and three oil feed orifice diameters. Ref.[14] states that the outer film land contributes to about 70% of the total damping; see Figure 1 for reference. Therefore, the predicted coefficients are scaled by a factor equaling (1.0/0.7) = 1.43 to obtain the damping of the whole ISFD. The predicted damping agrees well with the experimental one.

The change of orifice diameter is very effective to alter the damping coefficient when the end seals' clearance is small. For example, with a seal gap b_1=0.191 mm, the increase in orifice diameter from d_0=1.98 mm to $3d_0$= 5.94 mm reduces C by ~ 51%. However, for the damper with a large seal gap, $3b_1$=0.573 mm, the damping coefficient reduces by only ~ 15%.

On the other hand, when the inlet orifice diameter is fixed, d_0=1.98 mm, an increase in the end seals' gap, from b_1=0.191mm to $3b_1$=0.573 mm, greatly reduces the damping coefficient by ~ 88%. For a damper with $3d_0$, C reduces by ~ 78%. The results shows that the increase in the size of the inlet orifice weakens the *rule of thumb* relationship $C \sim 1/c^3$" [14].

Figure **9** shows the predicted added mass coefficient (M) vs. the end seals' clearance (b_1). An increase in the seal end gap (b_1) and in the orifice diameter greatly reduces M. The predicted M is too large compared to the experimental coefficient in [14], albeit both show a significant physical magnitude, 15 kg and larger. However, in a rotordynamic analysis, the added mass term is almost invariably neglected since it appears not to affect much the system "logdec".

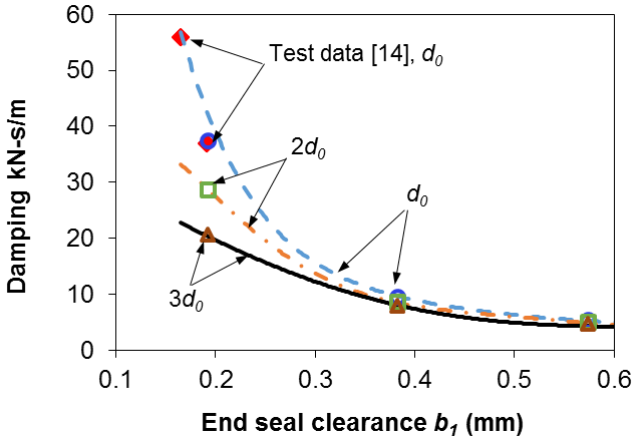

Figure 8 ISFD direct damping coefficient *C* vs. end seals' clearance b_1. Inlet orifice diameter = d_0, 2 d_0 , 3d_0. P_s=2.4 bar(a), P_a=1.0 bar(a). Lines: r_0=23 µm (r_0/c = 4%), Open symbols: r_0=56 µm (r_0/c = 10%), Solid symbols: test data from Ref. [14].

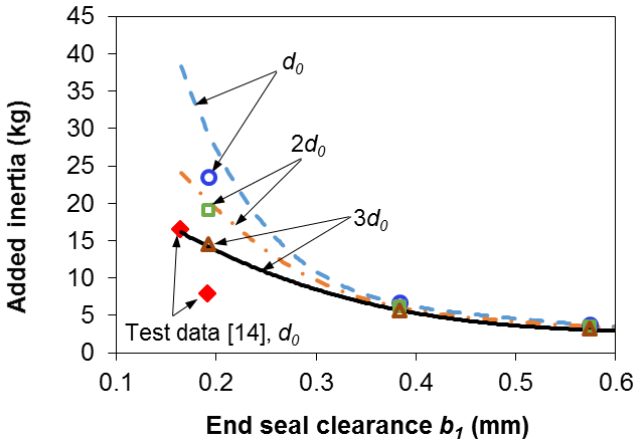

Figure 9 ISFD direct inertia coefficient *M* vs. end seals' clearance b_1. Inlet orifice diameter = d_0, 2 d_0 , 3d_0. . P_s=2.4 bar(a), P_a=1.0 bar(a). Lines: r_0=23 µm (r_0/c = 4%), Open symbols: r_0=56 µm (r_0/c = 10%), Solid symbols: test data from Ref. [14].

Figure 10 shows the direct damping C derived from Ima(H_{XX})/ω vs squeeze velocity (v_s=$r\omega$) and operation with orbit radii r/c = 0.04, 0.10 and 0.20. C is independent of the whirl motion for v_s < 0.22 mm/s. A further increase in v_s, due to either a larger r or a higher frequency ω or both, produces lubricant vapor cavitation in the film and thus a (linear) drop in the damping coefficient.

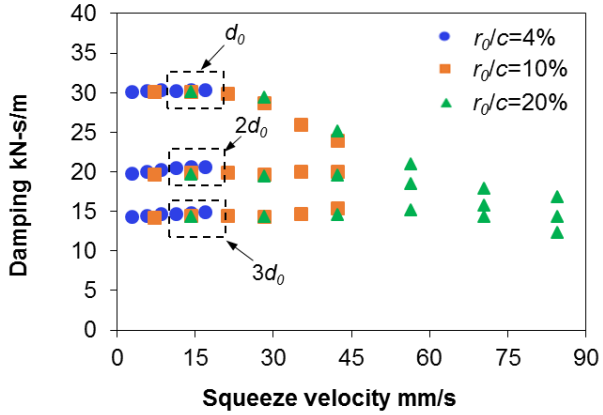

Figure 10 ISFD direct damping coefficients (*C*) vs squeeze film velocity (v_s=$r\omega$). Inlet orifice d_0 varies and end seals' clearance= b_1=0.191 mm. P_s=2.4 bar(a), P_a=1.0. Amplitude (r) and frequency (ω) of whirl motion varies.

San Andrés and Koo [19] analyze the dynamic force coefficients of a sealed ends SFD supplied with an air in oil bubbly mixture of known gas volume fraction at the inlet orifice. The experimentally derived and predicted damping coefficients decrease by ~20 % as the air volume fraction in the mixture increases to 50% while the inertia rapidly decreases.

Figure 11 and Figure 12 show the predicted force coefficients vs. inlet GVF for the current ISFD. The amplitude of whirl motion r_0=0.1c, and the peak squeeze velocity (v_s) is 42.2 mm/s. The end seals' clearance b_1=0.191 mm and the feed hole diameter equals d_0, 2 d_0 and 3 d_0. As the predictions show, both the direct damping and added inertia reduce continuously as the inlet GVF increases from 0 to 0.2. Note that the tests by San Andrés and Lu [24] for a bubbly seal also reveal that the damping and inertia coefficients reduces almost linearly with an increase in the GVF.

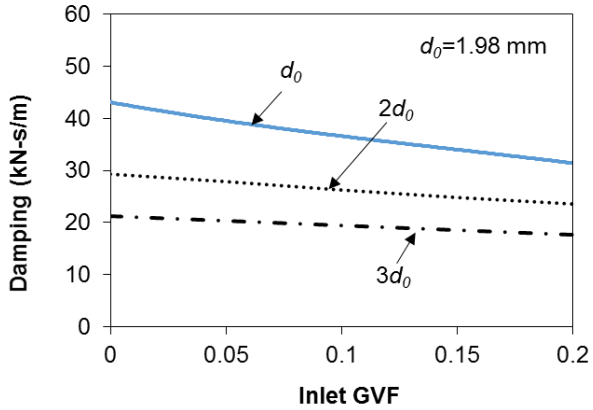

Figure 11 ISFD direct damping coefficient *C* vs. inlet GVF. Inlet orifice d_0=1.98 mm, end seal clearance b_1=0.191 mm. P_s=2.4 bar(a), P_a=1.0. Amplitude of whirl motion r_0=23 μm (r_0/c = 10%).

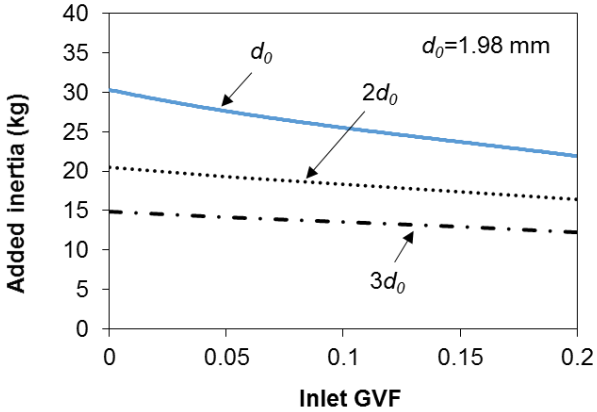

Figure 12 ISFD Predicted inertia coefficient *M* vs. inlet GVF. Inlet orifice d_0=1.98 mm, end seal clearance b_1=0.191 mm. end seal clearance b_1=0.191 mm. P_s=2.4 bar(a), P_a=1.0. Amplitude of whirl motion r_0=23 μm (r_0/c = 10%).

CONCLUSION

Squeeze film dampers (SFDs) help to reduce the amplitude of rotor whirl motions, provide structural isolation, and enhance system stability where rotor support bearings are inadequate to meet certain requirements. Compared to conventional squirrel cage supported SFDs, integral SFDS (ISFDs) provide a compact solution along with a short axial length. The lecture presented a physical model and predictions of flow rate and dynamic force coefficients for a four-arc pads ISFD supplied through orifices of increasing diameter d_0 to 3d_0. The damper has end seals with axial gap varying from b_1=0.191 mm to 3b_1. As the diameter of the feed orifice increase, so does the required flow rate, hence demanding of a larger oil reservoir.

Compared to the ISFD with inlet orifice diameter d_0, the damper having a seal clearance b_1=0.191 mm but supplied through larger orifices (2d_0, 3d_0) produces smaller damping and inertia coefficients. The magnitude of the damping and added mass coefficients generated by the ISFD with end seals having a tight clearance (b_1) is more sensitive to the feed hole diameter than to an increase in the end seals' clearance. An increase in the size of the inlet orifice weakens the *rule of thumb* for damping ~ 1/clearance^3 [14].

Predictions for the ISFD operating with an air in oil mixture show that the damping and inertia coefficients reduce almost linearly as the GVF increases from 0 to 0.2. Hence, air ingestion rapidly degrades the damper forced performance.

NOMENCLATURE

b_1	Gap or clearance of end plate seal [m]
C_f	Orifice (empirical) discharge coefficient [-]
c	Clearance [m]
e	Journal center dynamic displacement [m]
C	Damping coefficient [N.s/m]
D	Diameter of squeeze film section [m]
d_o	Feed orifice diameter [m]
F	Force [N]
H	Complex stiffness coefficient [N/m]
h	Film thickness [m]
L	Length
l_1	Radial length of end plate seal
M	Inertia coefficient [kg]
p	Film pressure [Pa]
P_s, P_a	Supply and ambient pressure [Pa]
q	Mass flow rate per unit length [kg/ms]
Q	Mass flow rate [kg/s]
r	Orbit radius amplitude [m]
v_s	($r\omega$). Squeeze (tangential) velocity [m/s]
(x,y)	Inertial coordinate system.
z	Axial coordinate
a	Gas volume fraction [-]
Θ	Circumferential coordinate [rad]
Θ_p	Pad arc extent [-]
μ	Oil viscosity [Pa.s]
ρ	Oil density [kg/m^3]
ω	Whirl frequency [rad/s]

Abbreviations

ISFD	Integral Squeeze film damper
SSV	Subsynchronous vibration
SFD	Squeeze film damper
TPJB	Tilting pad journal bearing

REFERENCES

[1] Zeidan, F. Y., San Andrés, L., Vance, J. M., 1996, "Design And Application Of Squeeze Film Dampers In Rotating Machinery," Proc. of the 25th Turbomachinery Symposium, Texas A&M University, Turbomachinery Laboratory, Houston, September, pp. 169-188, https://doi.org/10.21423/R1694R.

[2] Gunter, E., 2020, "Ekofisk Revisited-Bearing Optimization for Improved Rotor Stability," Dyrobes Rotordynamic Software, https://dyrobes.com/paper/ekofisk-revisited-bearing-optimization-for-improved-rotor-stability.

[3] Zeidan, F.Y., 1995, "Application of Squeeze Film Dampers," Turbomachinery International, pp. 50-53.

[4] Leader, M. E., Whalen, J. K., and Grey, G. G., 1995, "The Design and Application of a Squeeze Film Damper Bearing to a Flexible Steam Turbine Rotor," Proc. of the 24th Turbomachinery Symposium, Dallas, TX, pp. 49–58, https://doi.org/10.21423/R1R36D.

[5] Gooding, W.J., Meier, M.A., Gunter, E.J., and Key, N.L., 2020, "Nonlinear Response and Stability of an Experimental Overhung Compressor Mounted with a Squeeze Film Damper," ASME Paper No. GT2020-15212.

[6] Jeung, S.-H., San Andrés, L., Den, S., and Koo, B., 2019, "Effect of Oil Supply Pressure on the Force Coefficients of a Squeeze Film Damper Sealed with Piston Rings, ASME J. Eng. Gas Turb. Pwr., **141**, p. 061701.

[7] De Santiago, O., and L. San Andrés, 1999, "Imbalance Response and Damping Force Coefficients of a Rotor Supported on End Sealed Integral Squeeze Film Dampers," ASME Paper 99-GT-203, https://doi.org/10.1115/99-GT-203.

[8] Agnew, J., and Childs, D., 2012, "Rotordynamic Characteristics of a Flexure Pivot Pad Bearing with an Active and Locked Integral Squeeze Film Damper," ASME Paper No. GT2012-68564, https://doi.org/10.1115/GT2012-68564

[9] Ferraro, R., Catanzaro, M., Kim, J., Massini, M., Betti, D., and Hardy, R.L., 2016, "Suppression of Subsynchronous Vibration in

a 11 MW Steam Turbine Using Integral Squeeze Film Damper Technology at the Exhaust Side Bearing," ASME Paper GT2016-57410. https://doi.org/10.1115/GT2016-57410.

[10] Ertas, B., Cerny, V., Kim, J., and Polreich, V., 2015, "Stabilizing a 46 MW Multistage Utility System Turbine Using Integral Squeeze Film Bearing Support Dampers," ASME J. Eng. Gas Turb. Pwr., **137**, p. 052506.

[11] Saeki, K., Sanari, H., Baba, Y., Ito, M., Shibata, S., and Kurohashi, M., 2010, "Integrally Geared Centrifugal Compressors for High Pressure Process Gas Services," Kobelco Technology Review, No.29, Dec.2010. https://www.kobelco.co.jp/english/ktr/pdf/ktr_29/042-046.pdf

[12] Alford, J., 1965, "Protecting Turbomachinery from Self-Excited Rotor Whirl," ASME J. Eng. Power, **87**(4), pp. 333–343.

[13] Lerche,A.H., Musgrove, G.O., Moore, J.J., Kulhanek, C.D., and Nordwall, G., 2013, "Rotordynamic Force Prediction of an Unshrouded Radial Inflow Turbine Using Computational Fluid Dynamics," ASME paper No. GT2013-95137.

[14] Ertas, B., Delgado, A., and Moore, J., 2018, "Dynamic Characterization of an Integral Squeeze Film Bearing Support Damper for a Supercritical CO_2 Expander," ASME J. Eng. Gas Turb. Pwr., **140**(5), p. 052501.

[15] Lu, X., San Andrés, L., Koo, B., and Scott, T., 2021 "On the Effect of the Gap of End Seals on Force Coefficients of a Test Integral Squeeze Film Damper: Experiments and Predictions," ASME J. Eng. Gas Turb. Pwr., **143**(1), p. 011014.

[16] Zhang, J. X. and Roberts, J. B., 1996, "Force Coefficients for a Centrally Grooved Short Squeeze Film Damper," ASME J. Tribol., **118**(3), pp. 608-616.

[17] San Andrés, L., Koo, B., and Jeung, S.-H., 2019, "Experimental Force Coefficients for Two Sealed Ends Squeeze Film Dampers (Piston Rings and O-Rings): An Assessment of Their Similarities and Differences," ASME J. Eng. Gas Turb. Pwr., **141**(2), p. 021024.

[18] Iacobellis, V., Behdinan, K., Chan, D., and Beamish, D., 2020, "Effect of Hole Feed System on the Response of a Squeeze Film Damper Supported Rotor," Tribol. Int., **151**(2020), p. 106450.

[19] San Andrés, L., and Koo, B., 2020, "Model and Experimental Verification of the Dynamic Forced Performance of a Tightly Sealed Squeeze Film Damper Supplied With a Bubbly Mixture," ASME J. Eng. Gas Turb. Pwr., **142**, p. 011023.

[20] Delgado, A., and San Andrés, L., 2007, "A Model for Improved Prediction of Force Coefficients in Grooved Squeeze Film Dampers and Oil Seal Rings," ASME J. Tribol., **132(**3), p. 032202.

[21] Diaz, S., and San Andrés, L., 2000, "A Model for Squeeze Film Dampers Operating With Air Entrainment and Validation With Experiments," ASME J. Tribol., **123**(1), pp. 125–133.

[22] San Andrés, L, and Jeung, S.-H., 2016, "Orbit-Model Force Coefficients for Fluid Film bearings: A Step beyond Linearization," ASME J. Eng. Gas Turbines Power, **138**(2), p. 233502.

[23] Patel, V. P., and Coppins, D. G., 2001, "Selection of API 614, Fourth Edition, Chapter 3-General Purpose Lube Oil System Components for Rotating Process Equipment," Proc. of the 18th International Pump Users Symposium, Texas A&M University, Turbomachinery Laboratory, Houston, September. https://doi.org/10.21423/R1WT2C.

[24] San Andrés, L., and Lu, X., 2018, "Leakage, Drag Power, and Rotordynamic Force Coefficients of an Air in Oil (Wet) Annular Seal," ASME J. Eng. Gas Turb. Pwr., **140(1)**, p. 012505.

ACKNOWLEDGEMENT

The first author thanks Hunan SUND Technological Corp. for allowing publication of this paper.